Metrol. Meas. Syst., Vol. 32 (2025) No. 1, pp. 1–12
DOI: 10.24425/mms.2025.152776

PAN POLSKA AKADEMIA NAUK

METROLOGY AND MEASUREMENT SYSTEMS
Index 330930, ISSN 0860-8229
www.metrology.wat.edu.pl

M&MS

METHODOLOGICAL APPROACH TO THE MEASUREMENT OF BALL BEARING GROOVES GEOMETRIC PARAMETERS BASED ON COORDINATE MEASURING MACHINE

Chenghao Yu[1)], Dongyang Huang[2)]

1) Division of Mechanics and Manufacture Measurement Technology, Shanghai Institute of Measurement and Testing Technology, Shanghai, China (✉ *yuchenghao95@163.com*)
2) Materials Genome Institute, Shanghai University, Shanghai, China

Abstract

Bearings are essential components in aerospace machinery and various transportation vehicles, with the grooves inside them providing smooth tracks for rolling elements to carry loads while minimizing friction-induced wear. Accurate measurement of the dimensional and shape tolerances of these grooves is crucial. Coordinate measuring machines, known for their high precision and versatility, excel in measuring various types and shapes of workpieces. The bearing groove measurement method developed with CMMs introduces a notable innovation over conventional techniques. Unlike profilometers, which are often incapable of measuring certain groove types, this method can be applied to a broader range of samples, addressing a long-standing challenge. A comparison of uncertainty between this method and the traditional profilometer method resulted in an E_n value of 0.11, confirming its satisfactory measurement accuracy and compliance with the technical requirements for bearing groove geometric parameters.

Keywords: bearing grooves, coordinate measuring machine, profile gauge, uncertainty, E_n value.

1. Introduction

Bearings, pivotal in industries such as aviation [1–3], commercial spaceflight [4–6], automotive [7,8], and maritime [9,10] are indispensable components. Their failure can lead to catastrophic engine breakdown, underscoring the importance of their reliability. Bearings operating at high speeds typically encounter wear and spalling [11] as primary failure modes. Thus, optimizing the contact area between rolling elements (balls or rollers) and bearing components is crucial to facilitate smooth and unrestricted rolling of elements within the bearing assembly. Bearing grooves, specifically circular cross-section grooves of ball bearing races, undergo heat treatment before being processed using grinding and honing methods [12,13] to ensure precision. Accurate control over groove dimensions and shape errors is vital as it directly impacts the reliability and safety of aerospace equipment and transportation vehicles reliant on bearings. Furthermore, the shift towards lightweight design presents new challenges in terms of geometric errors and manufacturing processes for traditional components.

Article history: received August 24, 2024; revised October 18, 2024; accepted November 3, 2024; available online November 29, 2024.

The inner and outer rings of bearings are interconnected through grooves and rolling elements bearing the primary load at the contact points between the rolling elements and the bearing surface [14]. The dimensional parameters of bearing grooves play a pivotal role in their structural and mechanical performance, with parameters such as groove diameter and curvature radius significantly influencing the reliability of bearings during operation. Currently, metrology institutions commonly employ profile gauges for obtaining geometric parameters of bearing grooves through needle scanning. However, this method still poses certain limitations, particularly regarding the measurement accuracy of larger curvature radii. Industrial *Computed Tomography* (CT) utilizes X-rays to project images of objects under inspection, providing exceptional three-dimensional imaging and detailed internal analysis. It vividly, precisely, and visually illustrates the internal structure, material composition, and defects of the inspected object [15, 16], whereas practical measurement and evaluation encounter challenges due to the unique imaging principles and complex error sources inherent in Industrial CT. Additionally, the absence of high-precision size standards complicates the calibration of dimensional measurement traceability, with numerous factors affecting measurement accuracy.

Artificial intelligence has recently found application in the field of metrology, with the emergence of deep learning-based profile measurement methods [17] and bearing diagnosis techniques assisted by *convolutional neural networks* (CNNs) [18]. Deep learning has demonstrated the capability to achieve accurate three-dimensional reconstruction in certain measurement scenarios [17]. The robustness and anti-interference performance of CNNs in metrology can be significantly enhanced by optimizing hyperparameters and deep feature extraction [18]. Additionally, advancements in self-referenced interferometers [19] and autocollimators [20] have contributed to heightened accuracy in geometric measurements. Nevertheless, these novel methods often entail a high level of complexity. In experiments, reducing error through simple steps is desirable [21], and the uncertainty associated with independent parameters is critical for both data analysis and the evaluation of measurement methods [22]. Indirect measurements often introduce greater uncertainty, making direct measurement methods generally preferable. Therefore, the pursuit of an economical, efficient, accurate, and versatile measurement method, coupled with a rational analysis of measurement uncertainty, is crucial for achieving high-precision dimensional quality control of grooves. This, in turn, contributes to better meeting the metrological requirements of the bearing industry, ensuring product performance and quality. Various advanced coordinate measurement systems are widely popular in the precision manufacturing industry [23]. Here, we propose a novel measurement method based on a coordinate *measuring machine* (CMM) and conduct uncertainty analysis, demonstrating its compliance with technical requirements.

2. Measurement Method

The technical specifications of the bearing employed in the experiment specify a groove curvature radius of $R = 7.430 \pm 0.003$ mm. Considering its geometric configuration and the elevation of the targeted groove, various fixation methods were employed. The experimental samples were securely fastened onto the granite work platform of the coordinate measuring machine (Leitz Pmm544, Germany) using pressure plates, as illustrated in Fig. 1.

The aforementioned fixation methods are applicable to typical bearing standard parts. Nevertheless, for bearing components with distinctive structural characteristics or elevated measurement complexities, the capabilities of CMMs can be maximized. Auxiliary fixtures, in conjunction with the multi-probe approach, can be employed to rectify errors, thus improving accuracy while maintaining universality and repeatability.

Metrol. Meas. Syst., Vol. 32 (2025), No. 1, pp. 1–12
DOI: 10.24425/mms.2025.152776

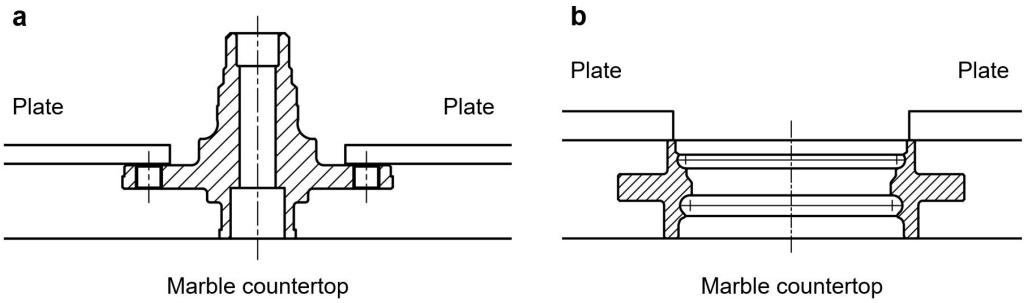

Fig. 1. Schematic of the fixation methods during the measurement of inner and outer bearing races. (a) Fixation method during inner race measurement; (b) Fixation method during outer race measurement.

During the measurement process, the standard part under examination is positioned flat on the worktable and firmly secured. Initially, the flat surface of the workpiece is measured, and coordinates are established. When measuring the curvature radius of the groove, the probe is manoeuvred to descend from the reference surface to the starting point of the groove circumference (which can be determined from drawings or observed visually). Subsequently, 6 to 8 points are uniformly collected along the arc of the groove, aiming to comprehensively cover the contour of the raceway (refer to Fig. 2).

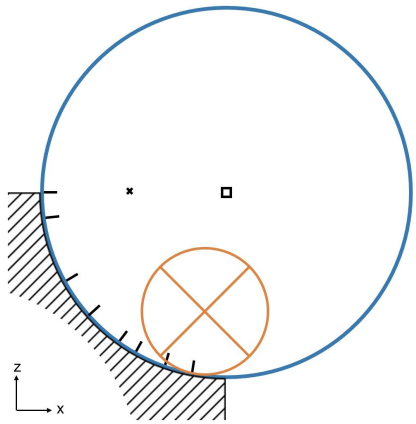

Fig. 2. Distribution of sampling points during measurement using a CMM. Small circles represent the ruby probe, while large circles represent the fitted groove shape.

After acquiring the measurement results, a least squares circle should be fitted to the data to determine the groove diameter/radius and roundness shape errors. To avoid introducing errors due to repeated manual measurements, the CMM should automatically conduct repeated measurements at different positions. This process enables the acquisition of data regarding the groove diameter/radius and roundness shape errors.

Upon completing the aforementioned measurement procedure, the workpiece should be horizontally rotated. Utilizing the CMM, the groove radius dimensions at the same positions should be measured in different directions following the same steps. By comparing the results obtained from different positions, the machining level of the groove can be evaluated. The complete experimental flow chart is presented in Fig. 3.

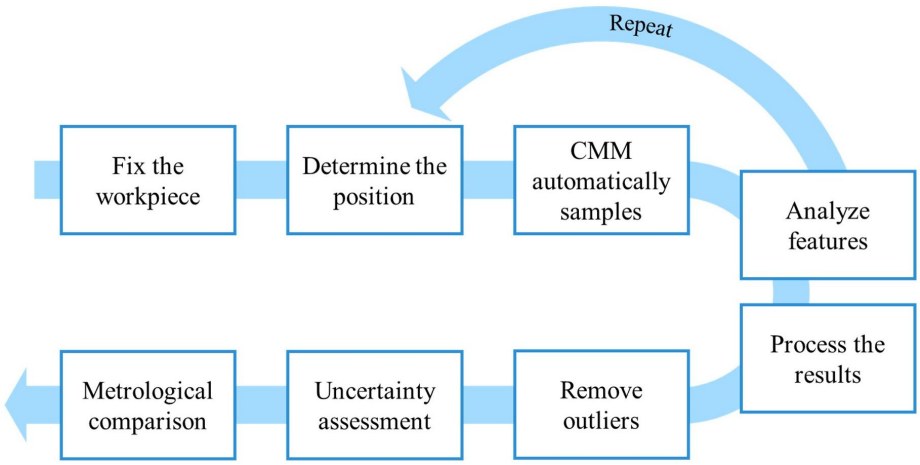

Fig. 3. Flow chart of the whole experiment.

3. Results and Discussion

3.1. Mathematical Model

This method employs direct measurement, meaning that the measured readings are equivalent to the actual measurement results. The mathematical model is as follows:

$$D = d \tag{1}$$

where D represents the distance from the centre of the groove circumference to the end face, d represents the measured distance value obtained by the CMM.

To evaluate the uncertainty propagation rate of the measurement, we calculate the sensitivity coefficient (ε):

$$\varepsilon = \frac{\partial D}{\partial d} = 1 \tag{2}$$

where $\frac{\partial D}{\partial d}$ represents the partial derivative of D with respect to d, which indicates how changes in the measured distance d affect the calculated distance D.

3.2. Standard Uncertainty Evaluation

The standard uncertainty (u_1) introduced by the precision of the CMM itself is evaluated using a non-statistical analysis method (Type B evaluation of measurement uncertainty) [24], as it cannot be obtained through repeated measurements. In Type B evaluation of measurement uncertainty, the ratio of half-width interval to distribution coefficient is used to calculate uncertainty [25, 26].

The maximum permissible error (tolerance) of the CMM used in this measurement is $\pm(0.8 + L/500)$ μm, where L represents the actual measurement size, i.e. in this case approximately 30.3 mm. Assuming a maximum error of 0.86 μm within a half-interval range according to a uniform distribution, the Type B uncertainty can be obtained using the following formula:

$$u_1 = 0.86\ \mu\text{m}/\sqrt{3} = 0.50\ \mu\text{m} \tag{3}$$

The standard uncertainty (u_2) arising from temperature differences is evaluated using a Type B evaluation method. During measurement, it is ensured that the test specimen is kept at a constant temperature in the laboratory for at least 24 hours, equilibrating with the CMM. The temperature difference is uniformly distributed within a range of $t_1 = \pm 0.3°C$. The test specimen is made of steel, and the linear coefficient of thermal expansion α_1 for steel is $(11.5 \pm 1) \times 10^{-6}$ m°C^{-1}. Thus, we can calculate u_2 as follows:

$$u_2 = \frac{1}{\sqrt{3}} c\alpha_1 t_1 = 0.16 \text{ µm} \tag{4}$$

where c is a parameter corrected for resolution of the displaying device and tolerance of the instrument, which is considered as 0.08 in our measurement.

The standard uncertainty (u_3) introduced by the difference in linear expansion coefficients is evaluated using a Type B evaluation method. The CMM used for the measurement employs an optical glass grating which has a linear expansion coefficient of $(10.5 \pm 1) \times 10^{-6}$ m°C^{-1}. The maximum difference $\Delta\alpha$ between α_1 and α_2 is 3×10^{-6} m°C^{-1}.

Assuming the difference in linear expansion coefficients is centred and the temperature deviates from 20°C by a maximum of $t_2 = 0.5°C$, we can calculate u_3 as follows:

$$u_3 = \frac{1}{\sqrt{3}} c\Delta\alpha t_2 = 0.07 \text{ µm} \tag{5}$$

The standard uncertainty (u_4) introduced by measurement repeatability is evaluated using a Type A evaluation method [24].

Following the measurement procedure outlined in Section 2, we conduct 10 repeated measurements of the groove radius at the same position on the sample using the CMM (Table 1). These measurements are performed automatically by the CMM in the measurement mode, yielding the following results (Fig. 4): 7.4313, 7.4317, 7.4312, 7.4314, 7.4313, 7.4312, 7.4315, 7.4313, 7.4316, 7.4313.

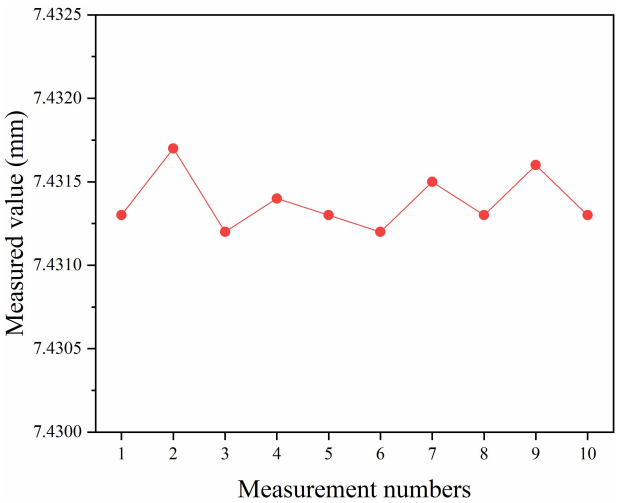

Fig. 4. Actual measurements obtained from 10 repeated measurements using the CMM.

The best estimate of this measurement is $\overline{x} = 7.4314$ mm (measurement results are rounded to four decimal places).

Table 1. Technical parameters of the CMM used in the experiment.

Equipment Name	Specification	Measurement Range	Accuracy	Manufacturer
Coordinate Measuring Machine	PMM544	X-axis: 0–500 mm Y-axis: 0–400 mm Z-axis: 0–400 mm	U = (0.8 + L/500) μm, L: mm, k = 2	Leitz (Germany)

According to Grubbs' criterion [27], we determine outliers in the 10 sets of measurement results. If there exists an outlier x_d among the repeated observations, it must satisfy the following condition:

$$\frac{|x_d - \overline{x}|}{s} \geq G(\alpha, N) \tag{6}$$

where s represents the experimental standard deviation of the measured data set, and $G(\alpha, N)$ represents the critical value of Grubbs' criterion, which depends on the sample size N of the measured results and is provided in Table 2.

Table 2. Critical values of Grubbs' criterion.

N	G (k = 2, α = 0.05)	G (k = 2.58, α = 0.01)
9	2.110	2.323
10	2.176	2.410
11	2.234	2.485

*k is the coverage factor.

The experimental standard deviation can be calculated using the formula:

$$s = \sqrt{\frac{1}{N-1}\sum_{i=1}^{N}(x_i - \overline{x})^2} = 0.90\ \mu\text{m} \tag{7}$$

The experimental standard deviation calculated using the formula is 0.90 μm. With a confidence level of p = 95%, we have α = 1− p = 0.05. Referring to the table, the corresponding critical value is $G(0.05, 10) = 2.176$. Substituting this into (6), we conclude that all results obtained from this measurement are valid, and no outliers exist.

3.3. Combined Standard Uncertainty

The summary of standard uncertainties for measuring the radius of bearing grooves using the CMM is presented in Table 3.

Since the above components are mutually independent, the combined standard uncertainty [28] is calculated as follows:

$$u_c(y) = \sqrt{\sum_{i=1}^{N}\left[\frac{\partial f}{\partial x_i}\right]^2 \cdot u^2(x_i)}, \tag{8}$$

Table 3. Sources of Standard Uncertainty Components.

Uncertainty Sources	u_i **(µm)**	**Sensitivity Coefficient**	**Corresponding Component (µm)**
The standard uncertainty (u_1) introduced by the indication error of the CMM	0.50	1	0.50
The standard uncertainty (u_2) introduced by temperature differences	0.16	1	0.16
The standard uncertainty (u_3) introduced by the difference in linear expansion coefficients	0.07	1	0.06
The standard uncertainty (u_4) introduced by measurement repeatability	0.90	1	0.90

where f is the measurement model, and in a mathematical model shaped like (1), f is equal to x_i. Expanding this expression, we get:

$$u_c = \sqrt{u_1^2 + u_2^2 + u_3^2 + u_4^2} = 1.04 \text{ µm}. \tag{9}$$

Taking the coverage factor $k = 2$, the expanded uncertainty of the measurement results of bearing groove dimensions using this method is:

$$U = ku_c = 2.1 \text{ µm} \tag{10}$$

3.4. Numerical Comparison

The radius of the bearing groove is typically measured using a profile gauge. However, the hardware performance of the probe in the profile gauge poses limitations. Poor repeatability of measurement results may occur when the groove depth of the test piece is large, the groove is positioned low, or the groove top surface obstructs the probe. Consequently, this can result in a large expanded uncertainty of the measurement results, making it challenging to meet usage requirements.

In contrast, employing a CMM for measurements offers a wider measurement range and is suitable for unique groove structures and positions that cannot be measured using conventional methods. Additionally, measurements can be performed at various positions.

To verify the measured data, the same bearing standard part as in Section 1 was measured (Fig. 5) using a profile gauge (Table 4) with a measurement range of 0 to 260 mm and an accuracy grade of $U = 0.5$ µm (with $k = 2$).

Table 4. Technical parameters of the profile gauge used in the experiment.

Equipment Name	**Specification**	**Measurement Range**	**Accuracy**	**Manufacturer**
Profile Gauge	LD260	0–260 mm	$U = 0.5$ µm, $k = 2$	Mahr (Germany)

Ten measurements were performed on the same outer race sample of the hub bearing, and the measurement results are as follows (Fig. 6): 7.4311, 7.4312, 7.4312, 7.4314, 7.4313, 7.4312, 7.4315, 7.4313, 7.4314, 7.4313.

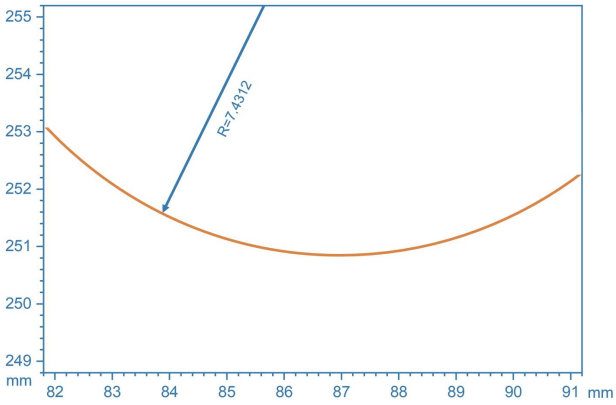

Fig. 5. Results obtained when using a profile gauge for measurement.

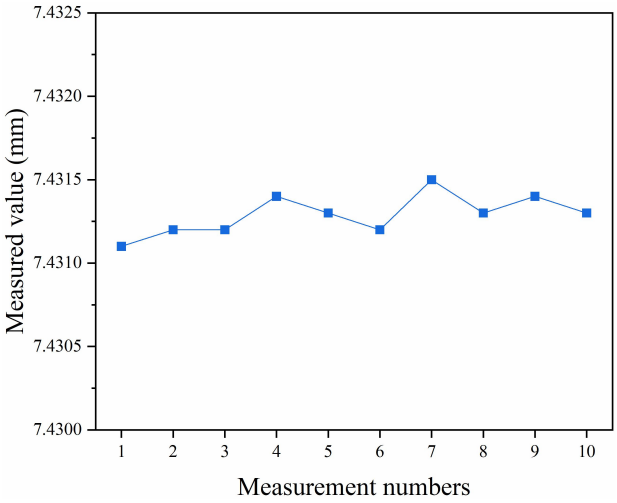

Fig. 6. Actual measurements obtained from 10 repeated measurements using the profile gauge.

The measurement results obtained from the CMM are compared with those obtained from the profile gauge. The comparison results are evaluated using the internationally accepted normalized error E_n value [29], where $|E_n| \leq 1$ indicates satisfactory results, and $|E_n| > 1$ indicates unsatisfactory results. E_n values are calculated using the following formula:

$$E_n = \frac{x - X}{\sqrt{U_{\text{lab}}^2 + U_{\text{ref}}^2}}, \tag{11}$$

where x represents the measurement result from the method under evaluation (test value), X represents the measurement result from the method being compared (reference value); U_{lab} is the expanded uncertainty of the measurement results from the method under evaluation, and U_{ref} is the expanded uncertainty of the measurement results from the profile gauge method.

The profile gauge measurement's expanded uncertainty (U_{ref}) for the groove radius is 1.0 μm. Combining this with Table 2 and Table 3, we obtain the comparison results (Table 5).

Table 5. Comparison Results.

Measurement Parameters	x	U_{lab}	X	U_{ref}	$\lvert E_n \rvert$
Groove Radius	R7.4314 mm	2.1 μm	R7.4312 mm	1.0 μm	0.11

From Table 5, it is evident that the comparison results $|E_n| \leq 1$, indicating that the measurement of the groove radius of the hub bearing component using the CMM in this study is correct, feasible, and the uncertainty assessment is reasonable. Additionally, the environmental conditions are suitable, and the comparison results are satisfactory.

4. Conclusion

With the widespread adoption of wide-body aircraft, commercial spaceflight, and new energy vehicles, along with the ongoing advancement of technology, the precision demands for bearings are steadily rising. Consequently, the need for inspecting various bearing components is diversifying and refining. The ball bearing groove measurement method proposed in this work has the following advantages:

1. As a direct measurement method, it introduces less uncertainty compared to indirect measurement approaches.
2. Compared to profilometer-based methods, the CMM-based approach demonstrates better applicability, enabling the measurement of complex bearing grooves that are beyond the capability of traditional profilometers.
3. The coordinate measuring machine, widely utilized across various applications, offers high precision and automation advantages.

This method, by leveraging the CMM to spatially position the groove location and measure the geometric parameters of bearing grooves through scanning or point acquisition, ensures high measurement accuracy. Moreover, it demonstrates adaptability, versatility, and high measurement efficiency.

The method proposed for measuring ball bearing grooves in this study addresses the limitations of traditional instruments in measuring bearing components. It expands the fault detection capabilities for bearing components and provides robust assurance for the application and development of bearings in the industrial field.

Future research in this field can focus on refining or integrating measurement methods to further enhance accuracy and reliability. The combination of artificial intelligence with traditional approaches also presents a promising avenue, as this emerging area offers both challenges and opportunities.

5. Nomenclature

CMM	coordinate measuring machine
R	radius, mm
D	the distance from the centre of the groove circumference to the end face, mm
d	the measured distance value obtained by the CMM, mm
ε	sensitivity coefficient
u_1	standard uncertainty introduced by the precision of the CMM, μm
u_2	standard uncertainty introduced by temperature differences, μm

u_3 standard uncertainty introduced by the difference in linear expansion coefficients, μm
u_4 introduced by measurement repeatability, μm
α_1 linear coefficient of thermal expansion for steel, m°C^{-1}
α_2 linear coefficient of thermal expansion for optical glass, m°C^{-1}
t_1 temperature range, °C
t_2 temperature deviates, °C
$\Delta\alpha$ maximum difference between $\alpha 1$ and $\alpha 2$, m°-1
$\overline{x}$ best estimate of measurement, mm
x_d outlier, mm
s experimental standard deviation
G critical value of Grubbs' criterion
N sample size of the measured results
u_c combined standard uncertainty, μm
f measurement model
k coverage factor
U accuracy grade, μm
x test value
X reference value
E_n normalized error
U_{lab} expanded uncertainty of the measurement, μm
U_{ref} expanded uncertainty of the measurement results from the profile gauge method, μm

References

[1] Zhang, S., Liu, Z., He, S., Wang, J., Chen, L. (2022). Improved double TQWT sparse representation using the MQGA algorithm and new norm for aviation bearing compound fault detection. *Engineering Applications of Artificial Intelligence*, *110*. https://doi.org/10.1016/j.engappai.2022.104741

[2] Li, Z., Wang, C., Hu, X., Xu, E., Yang, L. (2024). Thermal-Mechanical Coupling Performance and Its Influence on Thermal Stiffness of Cylindrical Roller Bearings. *Journal of Aerospace Engineering*, *37* (4). https://doi.org/10.1061/jaeeez.Aseng-5168

[3] Wang, B., Zhang, X., Sun, C., Chen, X. (2019). A Quantitative Intelligent Diagnosis Method for Early Weak Faults of Aviation High-speed Bearings. *ISA Transactions*, *93*, 370–383. https://doi.org/10.1016/j.isatra.2019.03.011

[4] Rejith, R., Kesavan, D., Chakravarthy, P., Narayana Murty, S.V.S. (2023). Bearings for aerospace applications. *Tribology International*, *181*. https://doi.org/10.1016/j.triboint.2023.108312

[5] Lorenz, S.J., Sadeghi, F., Trivedi, H.K., Kirsch, M.S. (2023). Investigation into rolling contact fatigue performance of aerospace bearing steels. *International Journal of Fatigue*, *172*. https://doi.org/10.1016/j.ijfatigue.2023.107646

[6] Kerrouche, R., Dadouche, A., Boukraa, S. (2023). Thermal characteristics of a 90-mm bore cylindrical roller bearings for aerospace applications: All-steel versus hybrid bearings. *Tribology International*, *185*. https://doi.org/10.1016/j.triboint.2023.108495

[7] Guo, H., Duan, H., Lei, J., Wang, D., Du, S., Zhang, Y., Ding, Z. (2021). Failure analysis of automobile engine pump shaft bearing. *Advances in Mechanical Engineering*, *13* (4). https://doi.org/10.1177/16878140211009411

[8] Li, W., Chen, Q., Yang, Y., Xiao, Y., Li, M. (2021). Investigation on clinching assembly process of automobile wheel hub bearings. *Proceedings of the Institution of Mechanical Engineers, Part D: Journal of Automobile Engineering*, *235* (8), 2114–2123. https://doi.org/10.1177/0954407020987912

[9] Soni, T., Dutt, J.K., Das, A.S. (2021). Magnetic Bearings for Marine Rotor Systems — Effect of Standard Ship Maneuver. *IEEE Transactions on Industrial Electronics*, *68*(2), 1055–1064. https://doi.org/10.1109/tie.2020.2967664

[10] Soni, T., Das, A.S., Dutt, J.K. (2020). Active vibration control of ship mounted flexible rotor-shaft-bearing system during seakeeping. *Journal of Sound and Vibration*, *467*. https://doi.org/10.1016/j.jsv.2019.115046

[11] Yang, L., Xue, W., Gao, S., Liu, H., Cao, Y., Duan, D., Li, D., Li, S. (2022). Study on sliding friction and wear behavior of M50 bearing steel with rare earth addition. *Tribology International*, *174*. https://doi.org/10.1016/j.triboint.2022.107725

[12] Chang, Z., Jia, Q. (2019). Optimization of grinding efficiency considering surface integrity of bearing raceway. *SN Applied Sciences*, *1* (7). https://doi.org/10.1007/s42452-019-0697-8

[13] Jiang, J., Ge, P., Sun, S., Wang, D. (2017). The theoretical and experimental research on the bearing inner ring raceway grinding process aiming to improve surface quality and process efficiency based on the integrated grinding process model. *The International Journal of Advanced Manufacturing Technology*, *93* (1–4), 747–765. https://doi.org/10.1007/s00170-017-0462-3

[14] Moazen Ahmadi, A., Petersen, D., Howard, C. (2015). A nonlinear dynamic vibration model of defective bearings – The importance of modelling the finite size of rolling elements. *Mechanical Systems and Signal Processing*, *52–53*, 309–326. https://doi.org/10.1016/j.ymssp.2014.06.006

[15] Yang, Z., Huang, Z., Zha, H., Zhou, L., Huang, K. (2023). Measurement uncertainty evaluation and analysis for industrial computed tomography based on forest balls. *Optics and Precision Engineering*, *31* (11), 1672–1683. https://doi.org/10.37188/OPE.20233111.1672

[16] Chen, Z.-m., Hu, Z.-w., Wang, Q.-n., Shi, Y.-w. (2020). Error and limit determination for dimensional measurements of thin-walled structures with industrial computed tomography. *Journal of Materials Engineering*, *48* (8), 169–176. https://doi.org/10.11868/j.issn.1001-4381.2019.000286

[17] Chen, Y., Kang, J., Feng, L., Yuan, L., Liang, J., Zhao, Z., Wu, B. (2024). Deep learning-based frequency-multiplexing composite-fringe projection profilometry technique for one-shot 3D shape measurement. *Measurement*, *233*. https://doi.org/10.1016/j.measurement.2024.114640

[18] Li, X., Ma, Z., Yuan, Z., Mu, T., Du, G., Liang, Y., Liu, J. (2024). A review on convolutional neural network in rolling bearing fault diagnosis. *Measurement Science and Technology*, *35* (7). https://doi.org/10.1088/1361-6501/ad356e

[19] Samuels, M.H., Kramer, A.R., Richardson, C.J.K. (2024). A self-referenced interferometer for in situ cryogenic wafer curvature measurements. *Review of Scientific Instruments*, *95* (4). https://doi.org/10.1063/5.0189541

[20] Eves, B.J., Leroux, I.D. (2023). Autocollimators: plane angle measurand ambiguities and the impact of surface form. *Metrologia*, *60* (6). https://doi.org/10.1088/1681-7575/acf9a8

[21] Sur, A., Das, R.K. (2017). Experimental investigation on waste heat driven activated carbon-methanol adsorption cooling system. *Journal of the Brazilian Society of Mechanical Sciences and Engineering*, *39* (7), 2735–2746. https://doi.org/10.1007/s40430-017-0792-y

[22] Roy, A., Kale, S., Lingayat, A.B., Sur, A., Arun, S., Sengar, D., Gawade, S., Wavhal, A. (2023). Evaluating energy-saving potential in micro-cold storage units integrated with phase change

material. *Journal of the Brazilian Society of Mechanical Sciences and Engineering*, *45* (10). https://doi.org/10.1007/s40430-023-04434-0

[23] Zhu, L., Zhao, M., Yang, S., Huang, Y., Jiang, H., Qin, X. (2024). Analysis and design of a novel target coding method for a portable coordinate measurement system. *Metrology and Measurement Systems*,*31*, 135–151. https://doi.org/10.24425/mms.2023.148535

[24] Wan, X.X., Huang, X.G., Liu, Z. (2010). Uncertainty Evaluation of Spectral Color Measurement. *Advanced Materials Research*, *174*, 36–39. https://doi.org/10.4028/www.scientific.net/AMR.174.36

[25] Shi, Y., Wang, W., Nie, X., Miao, J., Chen, W. (2024). Uncertainty analysis for free-space three-dimensional measurement of electromagnetic pulse. *Metrology and Measurement Systems*, *31*, 213–229. https://doi.org/10.24425/mms.2024.148547

[26] Dorozhovets, M. (2023). Uncertainty of the conversion function caused by systematic effects in measurements of input and output quantities. *Metrology and Measurement Systems*, 30, 581–600. https://doi.org/10.24425/mms.2023.146422

[27] Zhou, W., Xie, J., Xi, K., Du, Y. (2019). Modified cell averaging CFAR detector based on Grubbs criterion in non-homogeneous background. *IET Radar, Sonar & Navigation*, *13* (1), 104–112. https://doi.org/10.1049/iet-rsn.2018.5160

[28] Santo, M.D., Liguori, C., Paolillo, A., Pietrosanto, A. (2004). Standard uncertainty evaluation in image-based measurements. *Measurement*, *36* (3–4), 347–358. https://doi.org/10.1016/j.measurement.2004.09.011

[29] Steele, A.G., Douglas, R.J. (2006). Extending En for measurement science. *Metrologia*, *43* (4), S235–S243. https://doi.org/10.1088/0026-1394/43/4/s10

Chenghao Yu received his B.Eng. degree in mechanical and electronic engineering from Northwest A&F University in 2017 and his M.Eng. degree in mechanical engineering from Shanghai University in 2020. He is currently working as a Level 1 Certified Metrology Engineer at the Shanghai Institute of Measurement and Testing Technology. His research interests include the development of high-precision coordinate measuring machine standards, metrology for medical devices, metrology in the integrated circuit industry, and applications of artificial intelligence in metrological data processing.

Dongyang Huang received his B.Eng. degree in mechanical and electronic engineering from Northwest A&F University in 2017. Since 2019, he has been pursuing a Ph.D. degree in Materials Science and Engineering at Shanghai University and is expected to graduate from the Materials Genome Institute in 2025. His research interests include smart materials, materials physics, soft matter, flexible robotics, flexible electronics, smart devices, and applications of artificial intelligence in materials science.